Bull. Mater. Sci., Vol. 34, No. 2, April 2011, pp. 287–292. © Indian Academy of Sciences.

Synthesis and investigation of optical properties of ZnS nanostructures

NESLIHAN ÜZAR* **and M ÇETIN ARIKAN**
Physics Department, Science Faculty, Istanbul University, Vezneciler, 34134 Istanbul, Turkey

MS received 27 July 2010; revised 20 September 2010

Abstract. Structural characterizations of wurtzite zinc sulfide (ZnS) nanostructures synthesized by vapour–liquid–solid technique (VLS) were carried out by scanning electron microscopy (SEM), energy dispersive spectroscopy (EDS) and X-ray diffraction (XRD) analyses. Spectral dependence of photoluminescence (PL) was also carried out for optical characterization. PL results indicate that the bandgap energy of bulk ZnS which is 3·68 eV at room temperature changes from 3·7 eV to 3·72 eV depending on the size of the structures. We also supported these results by calculating the bandgap energies theoretically with using the infinite potential well approximation for 1D structures.

Keywords. ZnS nanowires; VLS; SEM; EDS; XRD; PL.

1. Introduction

Semiconductor nanostructures such as nanowires, nanobelts and nanoribbons have attracted great attention due to very high surface-to-volume ratio and their size-related quantum confinement properties, i.e. confinement of carriers by the boundaries of material when the material size is in nanoscale region. In this size regime as the material size becomes smaller, the semiconductor energy levels become more separated from each other and hence the effective bandgap increases. In addition, the electronic density of states in 3-, 2- and 1-dimensional systems vary as $E^{1/2}$, E^0 and $E^{-1/2}$, respectively. These effects lead to physical and chemical behaviours that are different from the bulk counterparts (Duan and Lieber 2000). They can be tuned and manipulated in fascinating ways by controlling the dimension. Therefore, these materials have wide range of potential applications including chemistry, physics, electronics, optics, materials science, biomedical science and nanodevices (Sun *et al* 1999; Kishimoto *et al* 2002).

ZnS, as a typical II–VI semiconductor compound with wide direct bandgap energy of 3·68 eV at room temperature, exhibits a wide optical transparency from the ultraviolet (UV) to the infrared (IR) region. This optical transparency combined with chemical and thermal stability makes ZnS one of the most widely used materials for optical windows. Discrete energy levels formed in the bandgap of ZnS by impurities and vacancies can be excited by illumination to produce PL behaviour that is utilized in electro-optic devices, such as flat panel displays. Its binding energy is 40 meV, which makes it an excellent candidate for exploring the intrinsic recombination processes in dense exciton systems. Moreover, ZnS is also widely used for laser, sensor (Jiang *et al* 2001), infrared windows, the cathode ray tube and electroluminescence device applications (Bredol and Merichi 1998; Calandra *et al* 1999). ZnS nanostructures can be synthesized using various techniques, such as solvothermal (Chen *et al* 2003), laser ablation (Jiang *et al* 2003a), liquid template (Xie *et al* 2000), sol–gel (Krumeich *et al* 1999) and VLS (Wang *et al* 2002; Li *et al* 2004), etc.

In this study, ZnS nanostructures were synthesized by the simple, rapid and low-cost VLS technique based on thermal evaporation of ZnS powders onto Si substrates covered by Au as catalyst. In this technique, the substrate temperature, concentration of ZnS vapour and flow rate of carrier gas are the critical experimental parameters to obtain ZnS nanostructures of different morphologies. The optical characterization of ZnS nanostructures was carried out using a PL measurement.

2. Experimental

The conventional VLS mechanism is based on evaporation of source material and transfer of vapour to lower temperature regions by using an inert gas as a carrier. The growth parameters are strongly dependent on the source temperature, substrate temperatures, the thickness of catalyst layer and the flow rate of carrier gas. Our experimental setup consists of a horizontal tube furnace (diameter 6 cm, length 78 cm) with a temperature control unit, a horizontal quartz tube (diameter 4 cm, length 150 cm), a quartz boat, a rotary vacuum pump, Au-coated Si substrates and Ar gas as the carrier gas with gas flow controlling system, as shown in figure 1(a).

*Author for correspondence (neslihanuzar@gmail.com, neslihanuzar@yahoo.com)

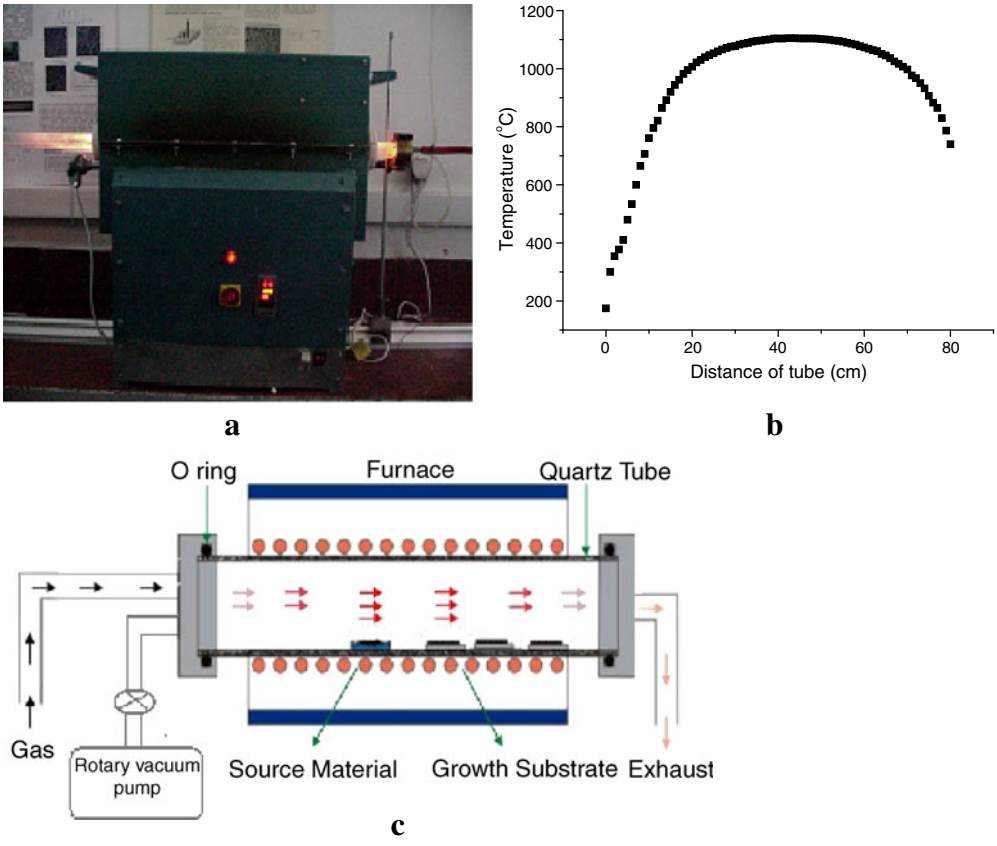

Figure 1. **a**. Experimental set up, **b**. temperature map of the furnace and **c**. schematical set up.

Before the experimental process started, the quartz tube previously placed in the furnace, heated up to 1100°C, below the sublimation point of bulk ZnS (sublimation point of ZnS, 1180°C) and the temperature distribution of the tube was obtained using a movable thermocouple (figure 1(b)) for the purpose of the substrates and the source material locations determination.

One terminal of the quartz tube was connected to a vacuum pump and the gas flow system. The quartz boat containing the source material (diameter 10 μm, 99·9% pure ZnS powder) and the Au-coated (50 Å) Si substrates were placed at the other edge of the quartz tube (figure 1(c)). Then the rotary vacuum pump evacuated the tube for 3 h. After closing the rotary pump, the tube was filled with high-purity Ar gas to eliminate any O_2 in the tube and the furnace was started to heat. When the furnace reached the process temperature (1100°C), the terminal opposite to the gas flow system opened and was kept open during the process for the gas to flow out. Then the quartz boat containing ZnS powder was transferred from edge of the tube to 1100°C temperature placed in the tube. The Au-coated Si substrates were placed at the pre-determined places having 850°C, 750°C and 600°C temperatures. Evaporated ZnS vapour was carried by 500 sccm of Ar gas and condensed on the substrates. After 90 min process, the quartz boat was taken off from the quartz tube rapidly. The Au-coated Si substrates were seen to be covered by white wool layers.

SEM and EDS analyses determine the surface morphologies and the chemical compositions of the synthesized structures, respectively. The crystal structure and the fine chemical compositions of the synthesized structures were investigated by XRD analysis (with Cu $K\alpha_1$ line). The PL measurement was carried out for optical characterization at room temperature. A mercury lamp with 253 nm filter was used as an excitation light, the luminescence from the surface of sample was directed through the monochromator and the dispersed light was collected using a photomultiplier tube (PMT).

3. Results and discussion

Figure 2(a) shows a typical SEM image of the nanostructures in the form of nanoribbons and nanowires mixture, synthesized at the 850°C temperature zone of the horizontal tube (hereafter called as ZnS_850). Our SEM observation demonstrates that the widths of the nanoribbons range from 250 nm to 450 nm and the diameters of the nanowires range from 80 nm to 150 nm. The lengths of both the structures can reach to approximately hundreds of micrometers

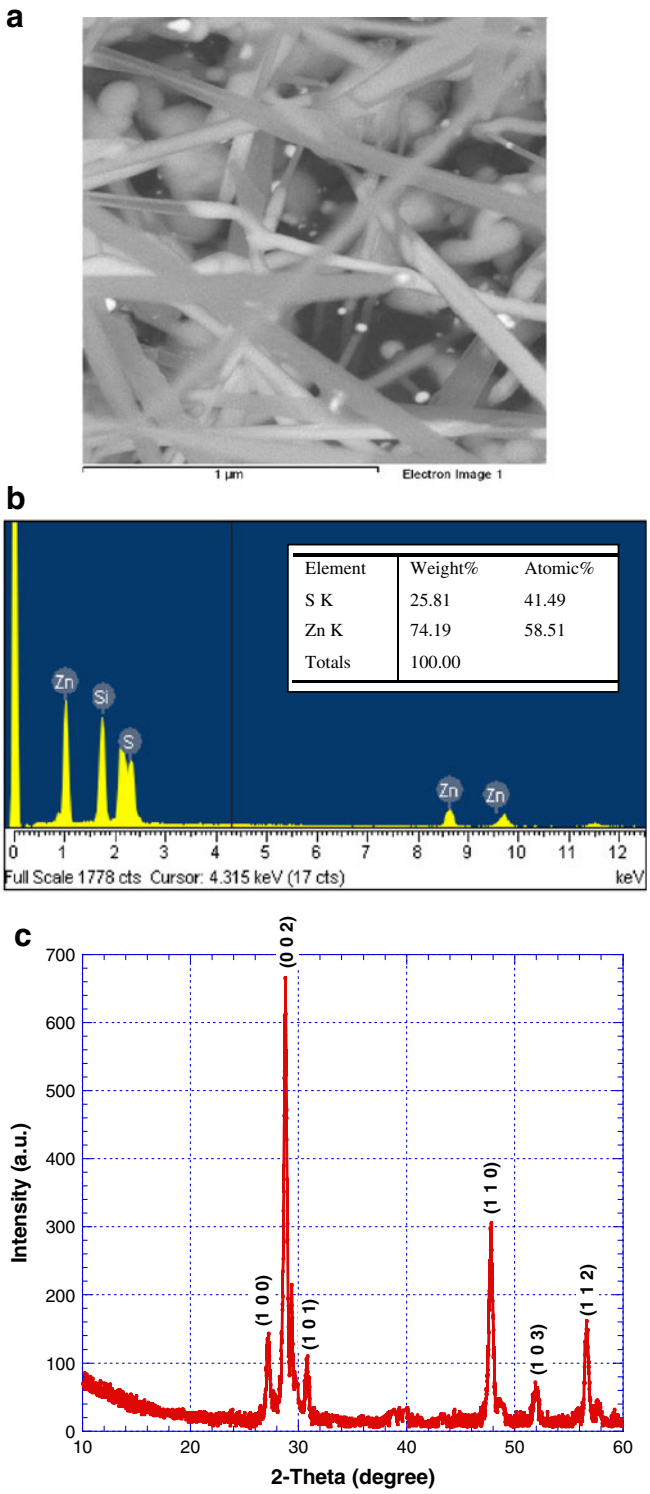

Figure 2. **a**. SEM image, **b**. EDS spectrum and **c**. XRD pattern of ZnS_850.

while the average thickness of the nanostructures is about 10 nm. Au nanodots are clearly seen at the tip of the nanostructures in SEM. The EDS analysis shows that the sample is composed of Zn and S elements as illustrated in figure 2(b). Atomic ratio of S in the sample is lower than that of

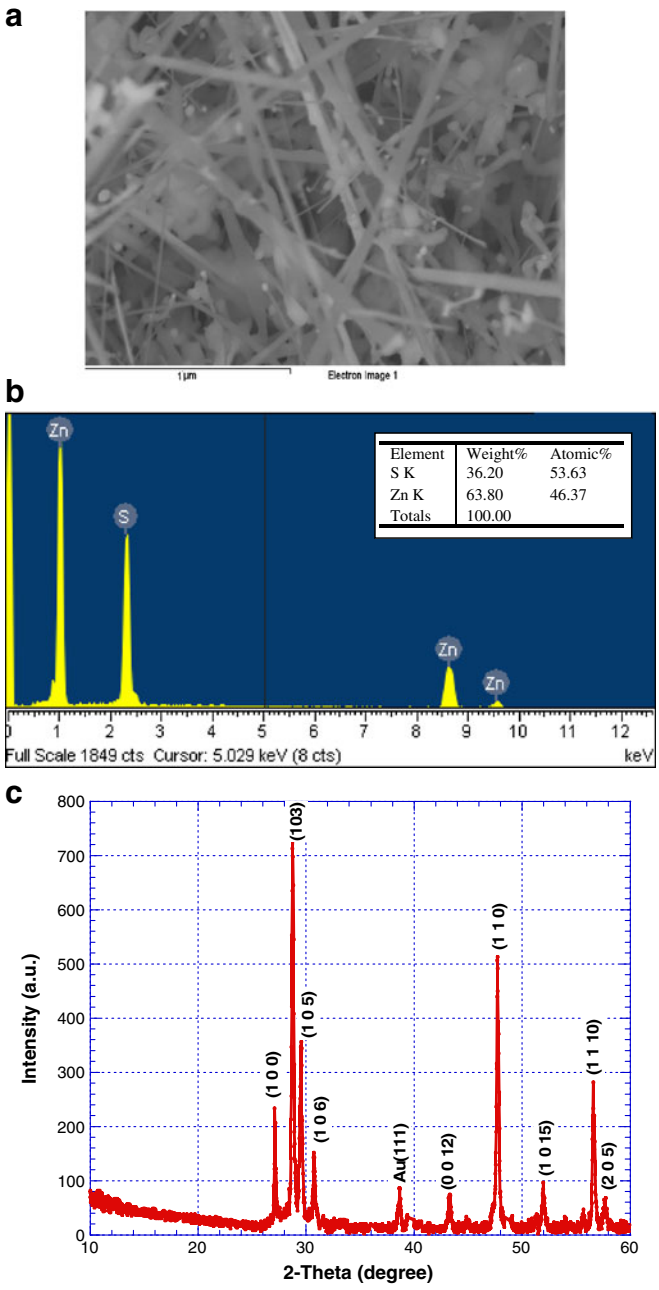

Figure 3. **a**. SEM image, **b**. EDS spectrum and **c**. XRD pattern of ZnS_750.

Zn element (S:Zn=41·49%:58·51%). The peak which is near the S peak belongs to Si element. Si peak in the EDS spectrum comes from the substrate, owing to very thin ZnS layer which formed on the substrate at high temperature point. Figure 2(c) shows the XRD pattern of ZnS_850. Diffraction peaks in the XRD pattern can be indexed to hexagonal (wurtzite)–2H crystal structured ZnS with lattice parameters of $a = 3{\cdot}82098$ nm and $c = 6{\cdot}2573$ nm, which matches well with the JCPDS card (36–1450).

Figure 3(a) shows the typical SEM image of the deposition layer on the surface of the Au-coated Si wafer placed at

the 750°C temperature zone in the tube (hereafter called as ZnS_750). SEM observation demonstrates that the substrate was densely covered with nanowires. The diameters of the nanowires are about 75–250 nm. The lengths of nanostructures can reach to several tens of micrometres and the average thickness of nanostructures is about 8 nm. The EDS spectrum in figure 3(b) shows that the atomic ratio of Zn and S is 46·37%:53·63% with low deviation from stoichiometry. In figure 3(c), the diffraction peaks in XRD pattern are indexed to hexagonal-10H structured ZnS with lattice parameters of $a = 3{\cdot}82$ nm and $c = 31{\cdot}2$ nm, which matches well with the JCPDS card (12–0688). Au peak which was seen in the XRD pattern is evident in VLS growth mechanism.

Figure 4(a) presents the SEM image of the structure synthesized at 600°C (hereafter called as ZnS_600). SEM observation demonstrates that only wire-like nanostructures formed and their lengths can reach to several tens of micrometers and their diameters change from 50 to 70 nm. The average thickness of nanowires is around 5 nm. The EDS analysis of ZnS_600 shows that the sample is composed of Zn and S elements, as illustrated in figure 4(b). The atomic ratio of Zn and S is nearly 47:53%. This elementary analysis shows that the synthesized structure is slightly zinc deficient. The XRD pattern in figure 4(c) indicates that the nanostructure could be formed of wurtzite-2H structured ZnS with lattice parameters of $a = 3{\cdot}82098$ nm and $c = 6{\cdot}2573$ nm, which matches well with the JCPDS card (36–1450).

We point out that the substrate temperature is the most important parameter to control the sizes and morphology of the products. The above-mentioned results indicate that low growth temperatures resulted in small diameters of ZnS nanostructures. Nanostructures start to become 2D, typically in the form of ribbon-like structures at high temperatures, i.e. at higher temperature ZnS crystal grew along the two optimized directions. At the start of condensation the lower energy side surfaces are formed. At high temperatures, the mobility of ZnS vapour increases and the side surface area expands. At slightly lower temperature, ZnS crystal structures generally grow along single direction to have the lowest energy states. In addition, thickness of catalyst can determine the size of nanostructures. The used Si substrates were Au-coated. Hence, the mismatch between the lattice constants of Au and Si can cause the formation of nanometer scale Au islands with temperature. At high temperatures, the sizes of islands can be larger than those of that formed at lower temperatures due to the increase in the kinetic energy of Au atoms and these small islands can coalesce with each other. This is reason why ribbon-like structures form. At the lower temperatures, structures generally grow along single direction to have the lowest energy states. We observed that the sample prepared at high temperature (850°C) has higher zinc or lower sulfur content compared to samples prepared at lower temperatures. The ZnS source material evaporates at 1100°C as Zn and S vapours. Zn and S vapours carry along with carrier gas to the low temperature zone, where they depose on the Au-coated substrate. Firstly,

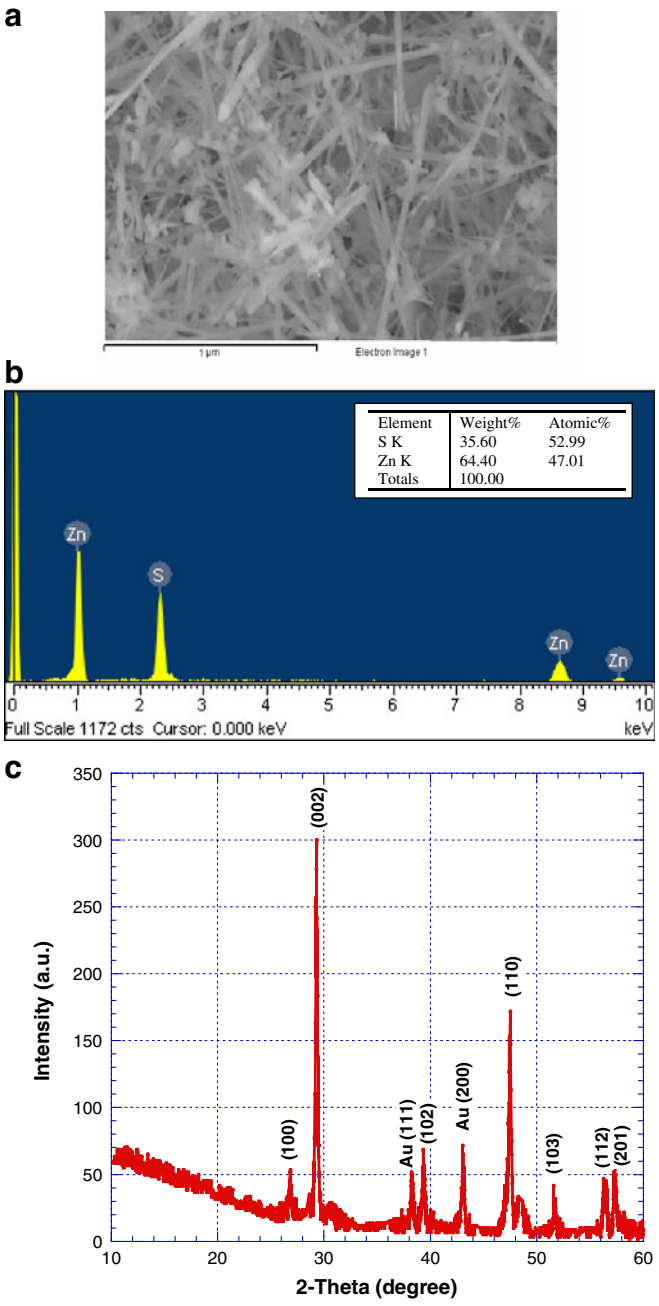

Figure 4. **a**. SEM image, **b**. EDS and **c**. XRD pattern of ZnS _600.

Au (Zn) liquid droplets form and these droplets would continuously absorb more Zn and S vapours from the carrier gas and inside the droplet Zn and S react again. As the concentration of ZnS reaches super saturation at the substrate temperature, ZnS phase would then separate out from droplet and form ZnS nanostructures. ZnS layer which was deposited on the substrate at 850°C was thinner than the samples prepared at lower temperature zone. The condensation which was on the substrate was very low at 850°C due to the high temperature. S is a more volatile element than Zn, i.e. sublimation point and pressure of Zn is higher than S and 850°C

is very high temperature for S element. Hence, condensation of S element on the substrate may not be easy and the amount of S atoms is lower than the Zn atoms. On the other hand, chemical bond between the Zn and S which are inside the droplet may break easily and S atoms may evaporate at high temperature zone. Due to these reasons, it is more possible to form structural defects at high temperature zone compared to lower temperature zone. Au peaks are seen in XRD patterns for samples prepared at 750 and 600°C but there is no trace of Au observed in EDS spectra due to different detection limits of XRD and EDS, i.e. data of XRD and EDS are taken from same sample but different regions of the sample. According to VLS mechanism, Au particles are at the tip of nanowires.

We also investigated the optical properties of ZnS_850, ZnS_750 and ZnS_600 with PL technique in air atmosphere and at room temperature. PL measurements then yielded information about bandgap energies of nanostructures that can be tuned by varying their sizes and the energetic positions of the electronic states in the bandgap. On the other hand, wide bandgap semiconductors are ideal materials for studies on trap states. Such localized states can be due to various types of imperfections like vacancies, interstitial atoms and dangling bonds. Bulk ZnS has a wide direct bandgap of 3·68 eV. The large exciton binding energy (40 meV) is much higher than thermal energy at room temperature (∼26 meV), the band edge PL of ZnS at room temperature is observed in high quality crystal. The typical PL spectra of these synthesized nanostructures are given in figure 5.

The black line in figure 5 shows the PL spectrum of ZnS_850. When only the green luminescence was observed from the sample with the naked eyes, the PL measurement shows three emission peaks at around 335 nm, 380 nm and 538 nm. PL emission peak at 335 nm (3·7 eV) corresponds to the bandgap energy of ZnS nanostructures (Jiang *et al* 2003b). The emission peak at 380 nm (3·26 eV) could be assigned to free-exciton recombination. The green emission at about 538 nm (2·3 eV) corresponds to the transition from the conduction band (3·7 eV) to the sulfur vacancies (V_S) level (1·4 eV) (Kurbatov *et al* 2009). Low concentration of S ions in ZnS which was given by EDS as shown in figure 2(b) causes large number of V_S. Sulfur vacancies can act as doubly ionized donor centres.

The red line in figure 5 shows the PL spectrum of ZnS_750. Three emission peaks are observed. The stronger two peaks are at around 334 nm, 373 nm and the weaker peak is at about 430 nm. The UV emission band, centred at 334 nm (3·71 eV) may show the band-to-band transition of ZnS nanowires. The intensive peak of PL spectrum at 373 nm (3·32 eV) can probably relate to the UV excitonic emission depending on exciton binding energy of 40 meV (Jiang *et al* 2003b; Li *et al* 2008). The blue emission at 431 nm (nearly 2·9 eV) is very weak and can be ascribed to either zinc vacancies (V_{Zn}) (Subbaiah *et al* 2007) or surface states (SS).

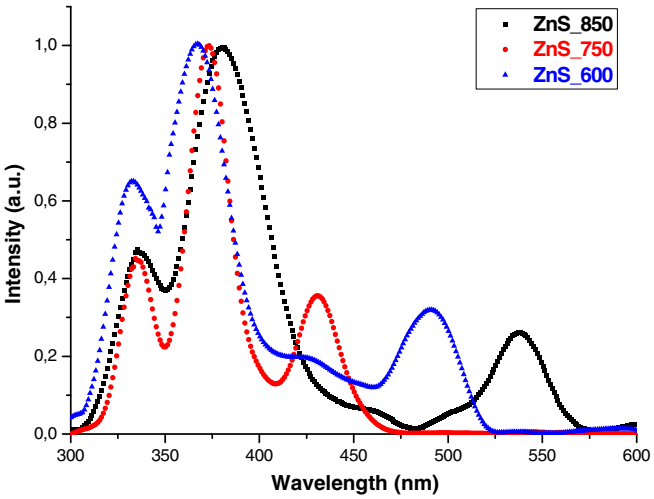

Figure 5. PL spectra of ZnS_850, ZnS_750 and ZnS_600.

The blue line in figure 5 shows the PL spectrum of ZnS_600. Three emission peaks are clearly observed at around 333 nm (3·72 eV), 367 nm (3·38 eV) and 491 nm (2·5 eV). According to the EDS analysis shown in figure 4(b), the atomic ratio of Zn is lower than that of S so that emission at 491 nm may be caused by the transition from the conduction band to the V_{Zn} level (this localized vacancy level is above the valence band at 1·1 eV). The peak at 368 nm (3·37 eV) can indicate exciton recombination. The peak at 333 nm (3·72 eV) in the UV region close to the bandgap energy of bulk ZnS (3·68 eV) may be the bandgap energy of ZnS nanostructures (Meng *et al* 2003).

The bandgap energies of ZnS_850, ZnS_750 and ZnS_600 are larger than that of bulk ZnS bandgap energy. Both excitonic emission energies and bandgap energies of obtained ZnS nanostructures increase with decreasing diameters of nanostructures. Beside transition band-to-band, the possible emission centres in a ZnS nanostructure can be related to surface/lattice defects (stoichiometric defects and interstitial impurities).

Increasing of bandgap energies of ZnS nanostructures could be an indication of the quantum confinement effect due to decreasing size of structures. In order to prove this idea, we calculated the effective bandgap energies using the infinitive quantum well approximation for 1D structure. The bandgaps of nanostructures can then be obtained by adding the bulk gap to the two confinement energies. The solution of this approximation is very simple.

The effective bandgap energy is given as

$$Eg_{\text{effective}} = Eg_{\text{bulk(ZnS)}} + E_{\text{e1}} + E_{\text{hh1}}, \tag{1}$$

where

$$\begin{aligned} E_{\text{e1}} &= \frac{h^2}{8m_{\text{e}}^* L_{\text{x}}^2} + \frac{h^2}{8m_{\text{e}}^* L_{\text{y}}^2}, \\ E_{\text{hh1}} &= \frac{h^2}{8m_{\text{h}}^* L_{\text{x}}^2} + \frac{h^2}{8m_{\text{h}}^* L_{\text{y}}^2}, \end{aligned} \tag{2}$$

Table 1. Calculation parameters with calculated and experimental bandgap energy of ZnS nanostructures.

Sample	Effective mass of electron for ZnS (m_e^*)	Effective mass of hole for ZnS (m_h^*)	Average thickness of structures ($\sim L_x$)	Average diameter of structures ($\sim L_y$)	Calculated $Eg_{effective}$	Experimental $Eg_{effective}$
ZnS_850	0·25 m_0	0·61 m_0	10 nm	150 nm	3·7 eV	3·7 eV
ZnS_750	0·25 m_0	0·61 m_0	8 nm	90 nm	3·71 eV	3·71 eV
ZnS_600	0·25 m_0	0·61 m_0	5 nm	60 nm	3·74 eV	3·72 eV

where m_e^* and m_h^* are the effective mass of electron and hole, respectively, h is the Planck constant, and L_x and L_y are the average thickness and diameter of the samples.

The value of parameters used in the calculations and the obtained results are given in table 1.

The calculated effective bandgap energies using the infinite potential well approximation for one dimension is well matched with the experimental effective bandgap energies. According to these results, the bandgap energy of the synthesized ZnS nanostructure is larger than that of bulk ZnS band energy (3·68 eV) due to the quantum confinement effect. Since the samples are not very thin their bandgap energy are close to that of bulk ZnS structure. In addition, vacancies and defects states in the bandgap of ZnS nanostructures may cause the emission in visible region.

4. Conclusions

In conclusion, semiconductor ZnS nanostructures have been successfully synthesized in bulk quantities by the simple low-cost process based on thermal evaporation of ZnS powders onto silicon substrates in the presence of Au catalyst. We found that the synthesized structures are ribbon and wire like, all having different sizes and diameters depending on substrate temperature. The UV emissions at 333 nm, 334 nm and 335 nm correspond to bandgap energies of ZnS_850, ZnS_750 and ZnS_600, respectively. The effective bandgap energies were calculated using the infinite quantum well approximation. The calculated bandgap energies are well matched with the experimental effective bandgap energies. According to both experimental and theoretical results, the bandgap energies of the synthesized ZnS nanostructure is larger than bulk ZnS band energy due to quantum confinement effect.

Acknowledgement

This study was financially supported by the Research Fund of the Istanbul University in Turkey (Project number T-676).

References

Bredol M and Merichi J 1998 *J. Mater Sci.* **33** 471
Calandra P, Goffredi M and Liveri V T 1999 *Colloids Surf.* **A9** 160
Chen X, Xu H, Xu N, Zhao F, Lin W, Lin G, Fu Y, Huang Z, Wang H and Wu M 2003 *Inorg. Chem.* **42** 3100
Duan X F and Lieber C M 2000 *Adv. Mater.* **12** 298
Jiang X, Xie Y, Lu J, Zhu L Y, He W and Qian Y T 2001 *Chem. Mater.* **13** 1213
Jiang Y, Meng X M, Lee C S and Lee S T 2003a *Adv. Mater.* **15** 195
Jiang Y, Meng X M, Lui J, Xie Z Y, Lee C S and Lee S T 2003b *Adv. Mater.* **15** 323
Kishimoto S, Kato A, Natio A, Sakamota Y and Tida S 2002 *Phys. Status Solidi* **B1** 391
Krumeich F, Muhr H J, Niederberger M, Bieri F, Schyder B and Nesper R 1999 *J. Am. Chem. Soc.* **121** 8324
Kurbatov D, Kosyak V, Opanasyuk A and Melnik V 2009 *Physica* **B404** 5002
Li J *et al* 2008 *Appl. Phys.* **A90** 759
Li M, Sudhiranjan T, Boothrayd C and Loh K P 2004 *Chem. Phys. Lett.* **400** 175
Meng X M, Lui J, Liang Y, Chen W W, Lee C S, Bello I and Lee S T 2003 *Chem. Phys. Lett.* **382** 434
Subbaiah Y P V, Prathap P, Reddy K T R and Miles R W 2007 *J. Phys. D: Appl. Phys.* **40** 5275
Sun L, Liu C, Liao C and Yan C 1999 *J. Mater. Chem.* **9** 1655
Wang Y, Zhang L, Liang C, Wang G and Peng X 2002 *Chem. Phys. Lett.* **357** 314
Xie Y, Huang J X, Li B and Qian Y T 2000 *Adv. Mater.* **12** 1523